

Received Date: 22-Dec-2016
Revised Date: 14-Jan-2017
Accepted Date: 16-Jan-2017
Article Type: Full Paper

Size Matters: Influence of Gold-to-Ligand Ratio and Sulfur-Sulfur Distance of Linear Thioether Heptamers on the Size of Gold Nanoparticles

Mario Lehmann^[a], Erich Henrik Peters^[a] and Marcel Mayor^{*,[a,b,c]}

[a] M. Lehmann, E. H. Peters, Prof. Dr. M. Mayor
Department of Chemistry
University of Basel
St. Johannis-Ring 19
4056 Basel, Switzerland
E-mail: marcel.mayor@unibas.ch

[b] Prof. Dr. M. Mayor
Institute for Nanotechnology (INT)
Karlsruhe Institute of Technology (KIT)
P. O. Box 3640
76021 Karlsruhe, Germany

[c] Prof. Dr. M. Mayor
Lehn Institute of Functional Materials (LIFM)
Sun Yat-Sen University (SYSU)
Guangzhou (P. R. China)

This article has been accepted for publication and undergone full peer review but has not been through the copyediting, typesetting, pagination and proofreading process, which may lead to differences between this version and the Version of Record. Please cite this article as doi: 10.1002/hlca.201600395

This article is protected by copyright. All rights reserved.

Abstract

A systematic investigation of two parameters steering the size of linear octadentate heptamers coated gold nanoparticles (AuNPs) is presented, being 1) the chemical structure (sulfur-sulfur distance) of the coating thioether heptamer ligand and 2) the ratio of ligand to tetrachloroauric acid (HAuCl_4) reduced during the formation of the AuNPs. For this purpose, a novel terphenyl-based thioether heptamer (**Ter**) is synthesized via an end-capping oligomerization strategy, comprising an increased distance between neighboring sulfur atoms in the ligand backbone compared to the *meta*-xylene- (**Xyl**) and tetraphenylmethyl- (**TPM**) based heptamers. While for both investigated parameters a clear trend to various-sized NPs is shown, a stronger influence in the resulting sizes is observed by alteration of ligand to gold-ratio. Remarkable processability- and long-term stability-features were observed for AuNPs stabilized by the bulky tetraphenylmethane-heptamer (**TPM**).

Keywords: gold; nanoparticles; S ligands; size control; oligomerization

Introduction

Since the seminal work of Brust and Schiffrin^[1] in the last century, the number of publications based on the synthesis of "small" nanoparticles (*i.e.* 1-10 nm) has been growing vastly.^[2] Within this small size regime, nanoparticles exhibit different electronic and optical properties^[3] which paved the way for new scientific fields of research. With sizes of 5 nm and below, gold nanoparticles (AuNPs) offer quantum dot like behavior^[4] or atom-mimicry features^[5] allowing their integration as stable building blocks^[6] in nanoelectronic devices.^[7,8] For sensing applications the size-trend goes into the opposite directions, benefiting from their optical properties offering larger plasmonic resonance bands (SPR).^[9-11] For this purpose, AuNPs should have diameters starting from at least 2 nm^[12], making them however more challenging to synthesize, especially if coated by a small integer number of ligands. Given these unique properties with different sizes, it is therefore imperative to be able to precisely control their sizes.

A concept for controlling the AuNPs size has been proposed by Hostetler and coworkers.^[13] They showed that by altering the molar ratio between the ligand (dodecanethiols) and the gold salt (HAuCl_4), and even the temperature or the rate at which the reduction is conducted, AuNPs between 1.5 to 5.2 nm can be synthesized. Since then, many different modifications of the two-phase Brust-Schiffrin method^[1] focusing on different sizes by altering ligand/Au ratio^[14-18] were published as well as by

This article is protected by copyright. All rights reserved.

altering the pH-value^[19,20]. In addition, the work of Hussain and collaborators shows that not only said ratio but the nature of the ligand itself can play a decisive role for resulting sizes, as different thioether polymers gave different sizes while maintaining the same reaction conditions.^[17] Recently McCaffrey et al. reported the first example of controlled AuNPs synthesis, templated in a well-defined, discrete organic cage with a size of 1.9 nm.^[21] Another example of cage-templated synthesis to stable and monodisperse NPs is reported by Mondal et al. with sizes up to 3.7 nm.^[22] While a recent study showed the mechanistic insights of the Brust-Schiffrin method for thiol derivatives^[23], the precise role of thioethers during the synthesis of AuNPs is a topic of current investigations.

Smaller sized nanoparticles (1.2 nm) are readily addressable by a small number of macromolecules like linear oligomers or dendrimers via multidentate thioether surface coating, as has been described -albeit scarcely- in literature.^[2] The weak interaction between a thioether moiety and the gold surface can amount considerable contribution by using multidentate oligothioether systems *e.g.* oligomers, and might even allow the macromolecule to self-rearrange for optimal conformation for the NPs coating. Inspired by this concept, we explored various multidentate macromolecules like linear oligomers^[24,25], and dendritic systems^[26] for the stabilization of small NPs. The low integer number of molecules per NPs decorated with a masked ethynyl moieties allowed mono- or bifunctionalized NPs to create supramolecular dumbbell^[27,28], trikes and quads^[28] or linear pearl-necklace^[29,30] hybrid materials via mild acetylene homo-coupling or acetylene/azide-click reactions. What is strikingly conspicuous however is the fact that all these macromolecule coated NPs feature almost the same sizes around 1-1.3 nm with barely noticeable SPR-bands (UV-Vis), and have thus limited potential for optical sensing applications. Note that the reaction conditions were kept as similar as possible throughout all the AuNPs-synthesis for better comparison along the different ligand structures. Even when comparing the dendritic ligands^[26] with a fairly prior determined cage-like form, and the linear ligands^[24,25] with no further predetermined curvature, the resulted NPs featured almost the same size. Also the spacing between the thioether sulfur atoms in the oligomeric ligand seems to have only a minor influence on the dimension of the stabilized nanoparticle, as demonstrated by the very comparable dimensions of nanoparticles stabilized by linear heptamers based either on a *m*-xylene-based motive^[29] and the more bulky tetraphenylmethane-based ligand^[25] with an increased spacing between the sulfur atoms. While the AuNPs showed promising stability features for both octadentate ligands, the major difference was the heptamer/NP ratio required, as two ligands of the xylene-derivative coated one NP while a single tetraphenylmethane-based ligand was able to enwrap an entire NP. These results were to some extent unexpected as with ligands based on pairs of interlinked thiophenols the dimensions of the stabilized

NPs reflected the ligand's inter-sulfur distances.^[31] We therefore wondered to which extent the ligand's design controls the dimensions of the formed NPs and perhaps the conditions under which the NPs are formed play a more important role with respect to the dimension of the formed AuNPs. We are interested in both, AuNPs enwrapped by a low integer number of capping macromolecules with distinct designs for potential functionalization at its periphery for further wet chemical applications. And on the other hand, NPs large enough exhibiting prominent SPR-bands suitable for optical sensing purposes. We thus decided to systematically vary the parameters space to investigate the ligands' correlation with the size of the obtained NPs. As parameters we focus in particular on the amount of used gold-salt during the AuNPs synthesis and on increasing the distance between sulfur-moieties by changing the ligand system, as sketched in Figure 1.

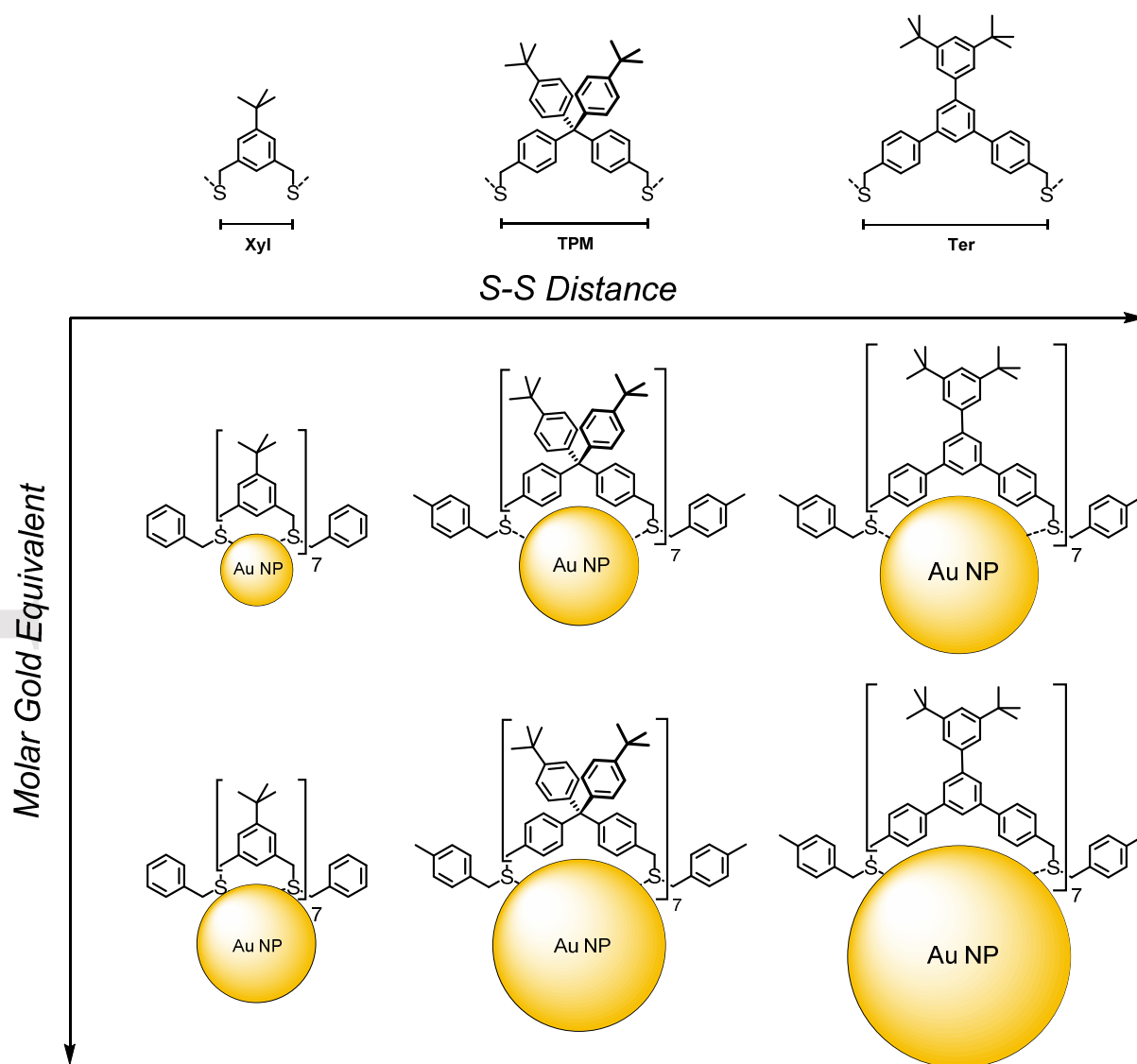


Figure 1: Representation of the two parameters potentially controlling the size of the formed nanoparticles. Namely the coating benzylic thioether heptamers with increasing sulfur-sulfur spacing from **Xyl** over **TPM** to **Ter**, and the molar amount of the gold formed during the nanoparticle synthesis. Note that heptamer **Xyl** was used with benzyl-groups as described in literature^[24] instead of 4-methylbenzyl as endcapping groups.

Here we report the systematic investigation of two parameters potentially steering the size of the thioether coated AuNPs. Namely the chemical structure of the coating thioether heptamer ligand and the ratio of ligand to the gold salt reduced during the formation of the AuNPs. Concerning the structure of the thioether ligands, the three different linear heptamers *m*-xylene^[24] (**Xyl**), tetraphenylmethane^[25] (**TPM**), and the newly designed terphenyl-type derivative (**Ter**) are studied.

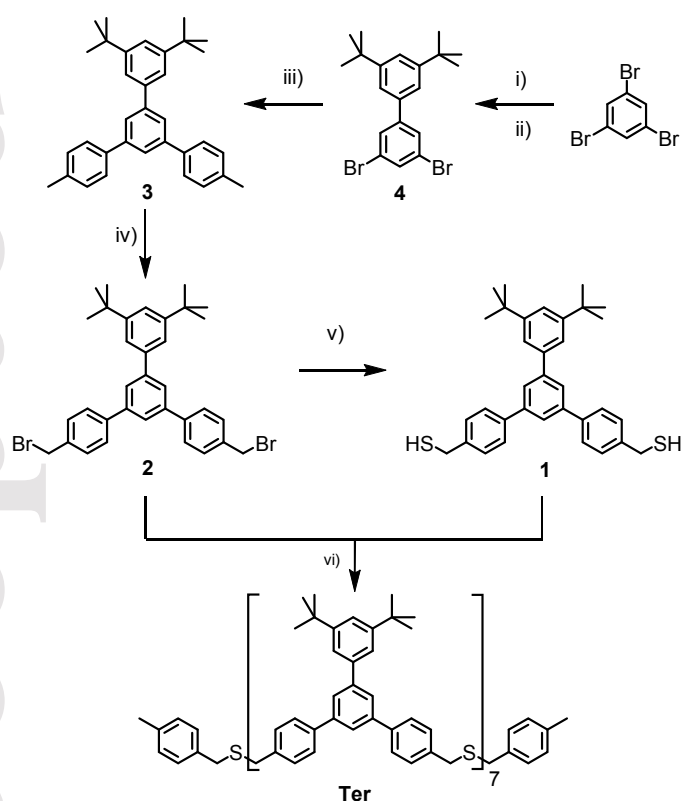
The molecular design of the terphenylic heptamer **Ter** comprises structural features with favorable features for the stabilization of AuNPs like the backbone's bulkiness provided by the 1,3-di-*tert*-butyl phenyl moiety mounted on the terphenyl linker. Furthermore, its increased spacing between both sulfur atoms (~12-14 Å) compared to the heptamers **Xyl** (~5-7 Å) and **TPM** (~10-12 Å)^[32] might provide insight into what extent the inter-sulfur bite-angle influences the dimensions of the formed particles. The increased spacing between neighboring sulfur atoms results in more remote contact points of the multidentate ligand on the AuNP's surface and thus might favor the stabilization of particles of alternative dimensions. However, as already mentioned for heptamer **TPM**, the increased spacing did not increase the resulting size of the AuNPs but altered the arrangement of the ligand on the particle's surface resulting in a new packing motif. This influence is hardly considered in literature^[31] for thioether moieties and will further be investigated with the new heptamer **Ter**, which was obtained by an end-capping oligomerization strategy followed by isolation via gel permeation chromatography (GPC). Another interesting feature will be the processability and long-term stability of the AuNPs coated with these three different ligand designs comprising each varying steric bulkiness.

Results and Discussion

Synthesis, Purification and Characterization

The synthesis of heptamer **Ter** (see Scheme 1) was performed *via* a one-pot end-capping oligomerization strategy with the advantage of making the entire family of oligomers in a single reaction and with the disadvantage that the individual members must be separated by chromatography. For this, precursors **1** and **2** were synthesized as follows: in the first step, mono-iodination of 1,3,5-

tribromobenzene was achieved following the protocol of Lustenberger and coworkers^[33] followed by a standard Suzuki-Miyaura protocol with 1,3-di-*tert*-butylphenylboronic acid in toluene and water giving compound **4** in yield of 60 % over two steps. Subsequent Suzuki coupling with **4** and *p*-tolylboronic acid in tetrahydrofuran (THF) and water gave compound **3** in 90 % yield. Bromination under mild conditions following the protocol of Peterle et al.^[24], with N-bromosuccinimide as bromine source and azobisisobutyronitrile (AIBN) as radical starter in refluxing methyl formate yielded the dibromine-precursor **2** in 90 %. Notably, the reaction had to be performed under argon atmosphere, as significant loss in yield is observed in the presence of quenching oxygen. The dibromine-precursor **2** was then treated with thiourea as sulfur source in dimethyl sulfoxide (DMSO) for 15 hours at 40 °C, and the reaction mixture was first hydrolyzed with an aqueous solution of sodium hydroxide and then protonated with aqueous hydrochloric acid, forming dithiol-precursor **1** in acceptable yield of 56 %. Heptamer **Xyl** and **TPM** were synthesized via the step-wise elongation/deprotection-strategy already reported in the literature.^[24,25]



Scheme 1: Molecular structures and synthesis towards precursors **1** and **2** and end-capping oligomerization reaction towards linear terphenyl-based thioether heptamer **Ter**. i) 1) *n*-BuLi, Et₂O, -78 °C → -20 °C, 1.5 h 2) I₂, -78 °C, 71 %; ii) (3,5-di-*tert*-butylphenyl)boronic acid, Pd(PPh₃)₄, K₂CO₃, toluene/H₂O, 90 °C, 15 h, 85 %; iii) *p*-tolyl boronic acid, Pd(PPh₃)₄, K₂CO₃, THF/H₂O, 80 °C, 24 h, 90 %; iv) N-bromosuccinimide (NBS), azobisisobutyronitrile (AIBN), methyl formate, hv, reflux, 90 %; v) 1) thiourea, DMSO, 40 °C, 15 h 2) DCM 3) 1 M aq. NaOH, 1 M aq. HCl, MeOH, 3 h, 56 %; vi) 1) NaH, THF, 15 min 2) 4-methylbenzyl bromide, 15 h, 8 %.

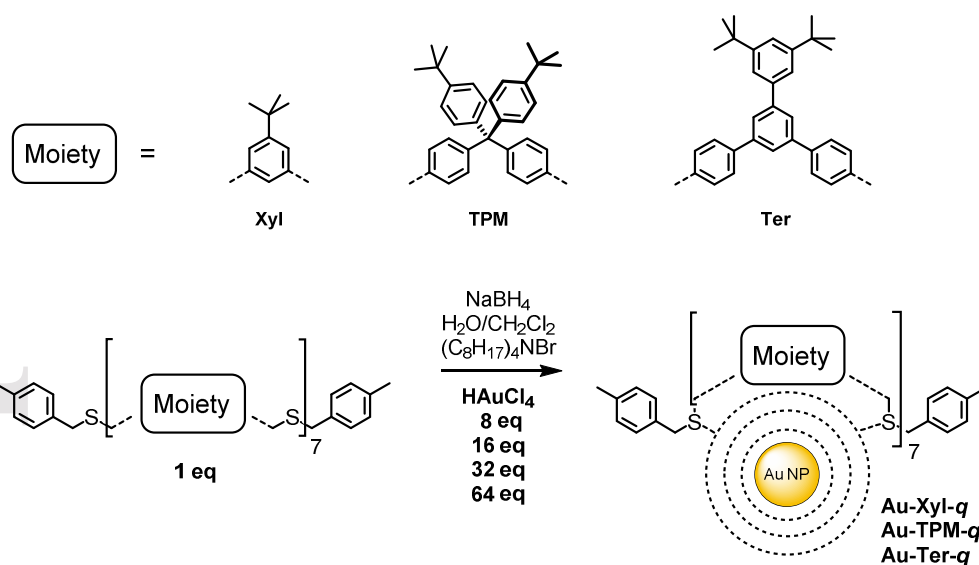
For the synthesis of the heptamer **Ter**, a one-pot end-capping oligomerization strategy via S_N2 reactions was elaborated. Note that this final end-capping oligomerization reaction only provides odd-numbered oligomers (1, 3, 5, 7 etc.) as the use of 4-methylbenzyl bromide as end-capping reagent defines the bis-

benzylthiol **1** as terminal building block trapped at both ends of the oligomer chain. Furthermore, the building of oligomers is expected to be sensitive to changes in stoichiometry, which enables the tuning towards a specific desirable oligomer. Since heptamer **Ter** consists of 7 building blocks (and two end-capping units), the reaction was performed with 4/3 molar ratio between the dithiol-precursor **1** (12.8 mM) and the dibromine-precursor **2** (10.3 mM). 4-Methylbenzyl bromide was chosen as end-capping unit due to its characteristic ^1H NMR signals simplifying the oligomers identification considerably. The protons residing on the methyl moiety as well as the upfield shifted AB-system recorded for the aromatic protons allows those signals to be used as internal standards to identify the particular member of the oligomer family by comparison of the integrals of the ^1H NMR signals. In a typical procedure, the reactants were dissolved in distilled THF and the reaction mixture was degassed with argon for 10 minutes (preventing major disulfide formations) before adding sodium hydride (NaH) as base to initiate the oligomerization. After 15 minutes, an excess of 4-methylbenzyl bromide (40.1 mM) as end-capping unit was added to prevent further oligomerization and the reaction mixture was kept stirring overnight at room temperature. After a quick workup and filtration, the heptamer was isolated via automated recycling GPC in chloroform as eluent. This separation technique is based on the separation of different molecules according to their hydrodynamic radii. In the present case, more than 24 hours were required to separate the heptamer from side products exhibiting very similar hydrodynamic radii, which are probably oligomers comprising disulfide linkages caused by oxygen residues present in the reaction mixture. However, extensive degassing of the reaction mixture for a longer period of time did not reduce the presence of these side products considerably. The heptamer **Ter** has been separated and purified successfully by this method in a yield of 8 %. Note that the addition of the end-capping unit in a later point of time (*i.e.* >15 min) did not increase the isolable yield, but increased the amount of side-products.

Nanoparticle Formation and Characterization

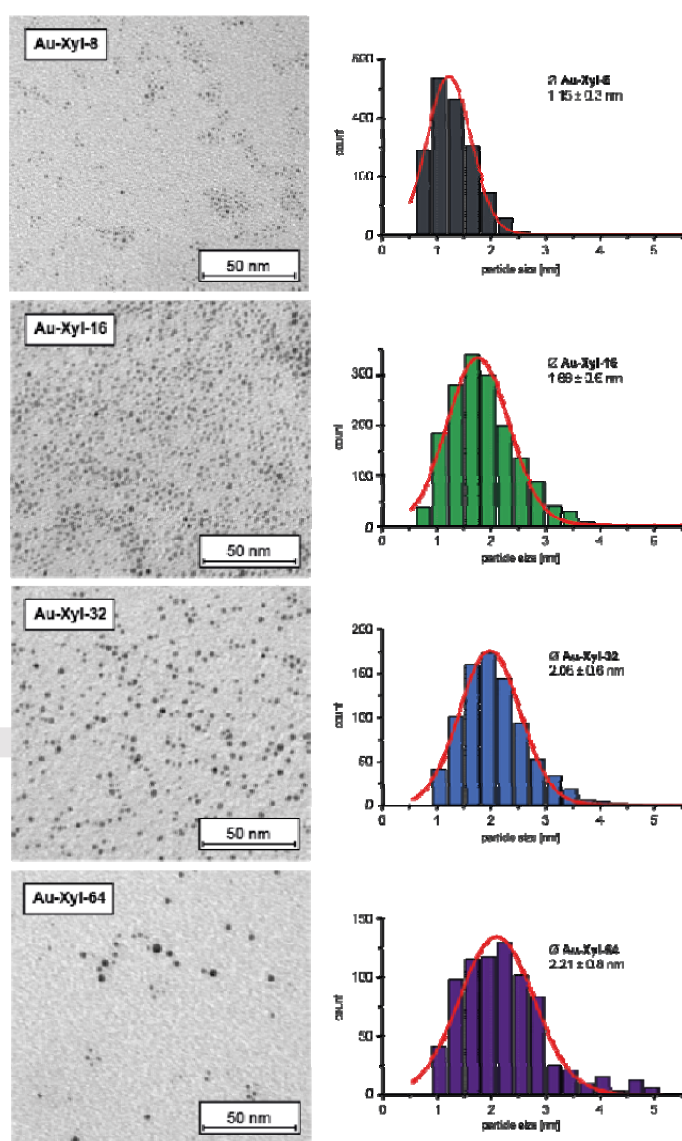
An adapted protocol of the two-phase Brust-Schiffrin method^[1] was used to synthesize AuNPs stabilized by the here investigated heptamers (**Xyl**, **TPM** and **Ter**, see Scheme 2). The main difference to our former studies on thioether stabilized gold nanoparticles^[24–30] was that the molar ratio of ligand to gold-salt was varied. So far we kept the growth conditions for the particles as uniform as possible enabling the comparison of stabilization features due to the ligands design and thus, a 1:1 molar ratio of thioether moieties to gold equivalents (e.g. 8 equivalents Au(III) per octadentate ligand) was used. In

this new study an exponential series of molar gold equivalents 8, 16, 32 and 64 (512 and 1024 only for heptamer **TPM**) was investigated to fully exhaust the scope of each ligand's stabilization ability. In a typical procedure, tetrachloroauric acid was first dissolved in deionized water, transferred to the organic phase upon addition of tetra-*n*-octylammonium bromide and stirred for several minutes until the completion of the phase transfer was indicated by a colorless aqueous phase. The ligand dissolved in DCM was then added to the reaction mixture. After 15 minutes, the reduction of Au(III) to Au(0) was triggered by addition of an aqueous solution of sodium borohydride (NaBH₄) to the two-phase system. For completion of the reducing process, stirring for another 15 minutes was required. As work up, the volume of the organic phase was reduced by steady stream of argon to approximately 0.5 ml and then centrifuged upon addition of ethanol. The supernatant was discarded and the precipitated particles were redispersed in dichloromethane and subjected to manual size exclusion chromatography (Biobeads SX1 in DCM) for the separation of excess ligand. The as-synthesized AuNPs were finally analyzed by UV-Vis spectroscopy, and transmission electron microscopy (TEM). For **Au-TPM-16**, **-32** and **-64**, which displayed the required stability as coated particles, their characterization was complemented by ¹H-NMR spectra and thermogravimetric analyses (TGA).



Scheme 2: Concept of AuNPs formation with the heptamers **Xyl**, **TPM** and **Ter** bearing different core length by varying the Lig/Au-ratio. Note that "*q*" is used for simplifying the names and corresponds to number of molar equivalents HAuCl₄ used for the reaction compared to one molar equivalent of ligand. Note that heptamer **Xyl** was used with benzyl-groups described in literature^[24] instead of 4-methylbenzyl as endcapping groups.

To clearly separate the influence of the different parameters we first discuss the development of the NPs sizes as a function of the gold equivalents used during their syntheses for each ligand system individually. And only in the second part the influence of structural features of the different ligand designs on the dimensions of the stabilized NPs will be compared.



AuNPs stabilized by heptamer Xyl

Figure 2: (Left) Representative sections of the TEM micrographs for samples of **Au-Xyl-8**, **Au-Xyl-16**, **-32** and **-64** and (right) their corresponding size distributions with calculated Gaussian curves (red). The vertical grid is implemented for better comparison.

Considering the synthesis towards AuNPs coated by heptamer **Xyl**, the more gold-salt used for the reaction (8, 16, 32 and 64 equivalents), the more reddish the solution appeared, while in the case of 16 equivalents still a dark brownish hue was visible similar to 8 equivalent of gold-salt used as reported by Peterle and coworkers.^[24] This reddish color already is a promising indication that larger NPs were formed with this octadentate ligand. Although during the progress of the synthesis for all entries comprising 16 equivalents or more of the gold salt, a black precipitation floating in the solution was observed by naked eye

while the intense color remained throughout the syntheses. The precipitation were insoluble agglomerates of coagulated NPs, which either pointed at a poor stabilization/protection of the NP provided by the surrounding ligand shell, or indicated that all ligands were already involved in the stabilization of the AuNPs and thus the remaining gold precipitates. The organic phases were then transferred into falcon tubes and the solvent was reduced to a volume of about 1 ml in a steady stream of nitrogen, followed by precipitation upon addition of ethanol and centrifugation. During this work up step potentially remaining excess of tetraoctylammonium bromide, which might also co-stabilize the AuNPs, was removed.^[34] The particles were further purified by manual gel permeation chromatography (GPC, Biobeads SX1 eluted with DCM) to remove potentially remaining excess of ligand. On the GPC column the NP samples obtained by applying 16, 32 or 64 gold equivalents smeared which is indicative for a limited stabilization of the NP by the ligand shell. Another indicator for the rather poor stabilization provided by the ligand was the fact that these NPs could no longer be redispersed after several drying/redispersing attempts. This poor processing behavior also made their characterization by ¹H-NMR spectroscopy and TGA impossible. To still analyze these NPs, the solutions were directly used to perform UV-Vis spectroscopy and to prepare samples suitable for transmission electron microscopy (TEM) analyses. TEM analysis (see Figure 2) shows for **Au-Xyl-8** a size of 1.15 ± 0.3 nm,^[24] **Au-Xyl-16** a size of 1.86 ± 0.6 nm (1.62 x), for **Au-Xyl-32** a size of 2.06 ± 0.6 nm (1.11 x) and for **Au-Xyl-64** a size of 2.21 ± 0.8 nm (1.07 x). This increasing dimensions of the NPs shows that the size is dependent on the ratio between the ligand and gold-salt. Probably as a consequence of the increased sizes, a clear trend to wider size-distributions with larger NPs is observed with **Au-Xyl-64** featuring a broad variation of ± 0.8 nm compared to the rather narrow distribution of ± 0.3 nm recorded for **Au-Xyl-8**. While **Au-Xyl-8** are enwrapped by two ligands per particle^[24], more ligands are probably involved in the stabilization of the larger NPs. While heptamer **Xyl** with the *meta*-xylene derivatives showed very promising stabilization features for the 1.15 nm-sized NPs, this was obviously less the case for larger NPs. Most likely the rather slim backbone of the octadentate heptamer **Xyl** exposing a single *tert*-butyl group per linking unit can neither be arranged in a compact coating covering the NPs surface efficiently nor provide sufficient steric repulsion to separate larger NPs.

AuNPs stabilized by heptamer TPM

During the AuNPs synthesis with heptamer **TPM** no precipitation was detected when 16 and 32 equivalents of gold-salt were used and only in the case of 64 equivalents a few black pieces were observed, but far less than while during particle synthesis with heptamer **Xyl**. This already shows at this stage, that the bulkier tetraphenylmethane-based ligand provides a thicker and therefore better protection shell covering the nanoparticles compared to the heptamer **Xyl**. The colors observed during

the synthesis were very similar to the ones observed during the syntheses described above using **Xyl** with comparable equivalents of the gold salt, pointing at comparable sizes of the stabilized NPs. Also during the subsequent purification by precipitation and redispersion cycles and GPC no signs of particle coagulation were observed for the **TPM** coated NPs. In contrast to the **Xyl** coated NPs, the GPC column charged with **TPM** stabilize NPs remained white pointing at complete wash-out of the particle fractions from the column, further corroborating the excellent stability features of the **TPM** coated particles. Indeed, the as-synthesized **Au-TPM-16**, **-32** and **-64** were stable enough for further processing, allowing in particular repetitive drying and redispersion. Therefore, additionally to TEM and UV-Vis analysis, TGA, $^1\text{H-NMR}$ and thermal-stability experiments were successfully performed (see supporting information).

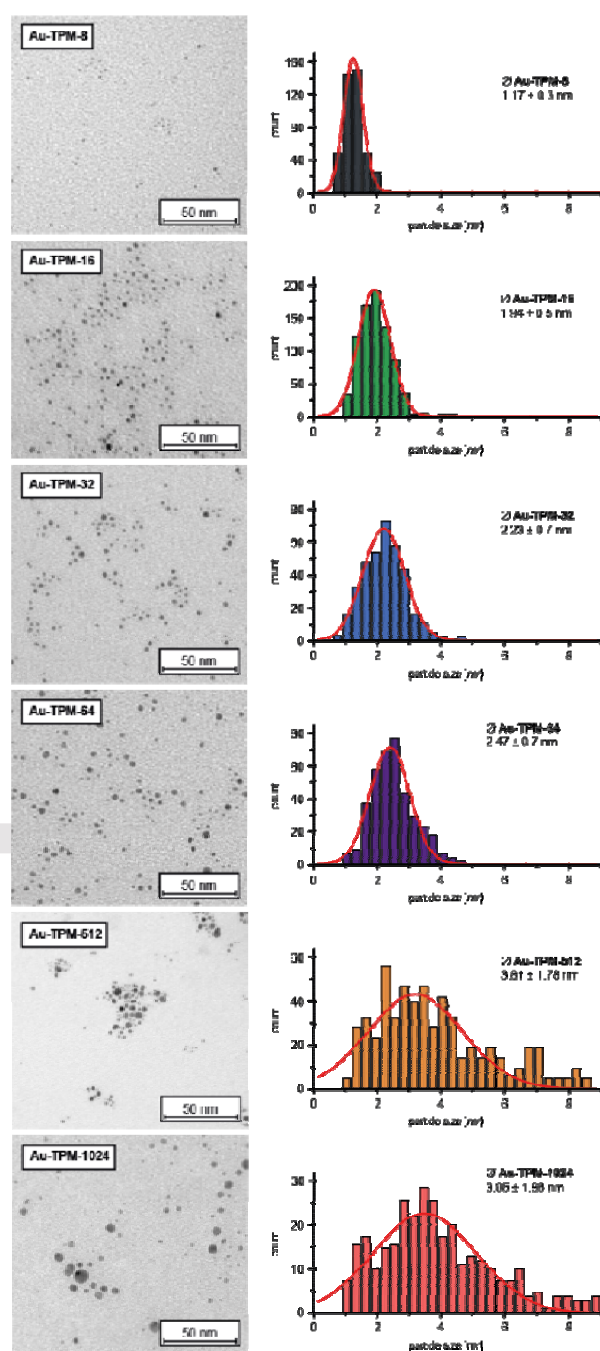


Figure 3: (Left) Representative sections of the TEM micrographs for samples of **Au-TPM-8, -16, -32, -64, -512** and **-1024** and (right) their corresponding size distributions with calculated Gaussian curves (red). The vertical grid is implemented for better comparison.

The ideal behavior of the heptamer **TPM** in the syntheses up to 64 equivalents of gold salt per thioether (8 equivalents per ligand **TPM**) raised questions concerning the limits of its stabilization ability. In order to explore the limit of the stabilization features of **TPM** we performed additional AuNP syntheses with 512 and 1024 molar gold equivalents. For these two NP syntheses considerable amounts of precipitates were detected in the dark red solutions. And in similarity to the larger AuNPs stabilized by heptamer **Xyl** described before, the **TPM** stabilized AuNPs obtained by using excessive amounts of gold salt were no longer dispersible after purification by GPC. The dimensions of the **TPM** coated AuNPs obtained from the various reaction conditions were again analyzed by TEM and the analyses are displayed in Figure 3. With diameters of 1.17 ± 0.3 nm for **Au-TPM-8**,^[25] 1.94 ± 0.5 nm for **Au-TPM-16**, 2.23 ± 0.7 nm for **Au-TPM-32**, 2.47 ± 0.7 nm for **Au-TPM-64**, 3.81 ± 1.8 nm for **Au-TPM-512**, and 3.95 ± 1.9 nm for **Au-TPM-1024** a similar trend to larger NPs and broader size distributions with increasing equivalents of the gold salt deployed during the synthesis was observed. As first approximation the diameter of the NP is expected to grow with the third radical of the mass, and thus, an increase of the particle diameter by the factor $\sqrt[3]{2} = 1.26$ would be expected for doubling the amount of gold equivalents. The observed increases in dimensions of successive NP syntheses from **Au-TPM-8** to **Au-TPM-64** were with 1.66, 1.15, and 1.11 within the expected dimensions but also point at alternative boundary conditions, like the dimension and the structure of the oligomer present, which control the sizes of the NPs. For the two samples prepared with excessive amounts of gold salt **Au-TPM-512** and **Au-TPM-1024** the observed increase was less than expected. **Au-TPM-512** was only 1.58 times larger than **Au-TPM-64** and **Au-TPM-1024** was only 1.01 times larger than **Au-TPM-512**, while increases by factors 2 ($= \sqrt[3]{8}$) and 1.26 respectively would have been expected. The lack of increase might be rationalized by the loss of gold during their syntheses by precipitation. However, the size distributions of these two samples was very broad further questioning the level of size control remaining during these reaction conditions.

¹H-NMR spectra (see Figures S1-S3) of **Au-TPM-16, -32, -64** showed the characteristic broadening of the signals (aliphatic and aromatic) in comparison to the pure ligand.^[24] The signals appear rather weak and might arise from the enlarged nanoparticles. However only a small amount of ligand was used in each case for the synthesis of the AuNPs compared to the enormous amounts of gold. Thermogravimetric analysis (see Figure S15-S17 and Table S1 for calculations in the supporting information) revealed an

increased amount of ligands per particle participating in the stabilization with increasing size of the NP. While **Au-TPM-8** with a size of 1.17 ± 0.34 nm is enwrapped in average by a single heptamer,^[25] the weight loss during the thermogravimetical analysis pointed at two (1.96) and three (2.96) heptamers which are in average stabilizing **Au-TPM-16** and **Au-TPM-64**, respectively. That the ratio between coating ligand and NP is no longer strictly an integer but that we encounter NPs stabilized by different numbers of ligands is displayed by **Au-TPM-32**, for which an average ratio between heptamer and NP of 2.33 has been recorded.

Another important factor for AuNPs is their thermal stabilities in suspension, limiting the range of potentially applicable reaction conditions. For this purpose, suspensions of the particles **Au-TPM-16**, **-32**, **-64** dispersed in toluene were gradually heated stepwise by 10 °C and kept at the elevated temperature for one hour before the integrity of the sample was analyzed by UV-Vis spectroscopy (see Figures S18-S20). For **Au-TPM-16**, no decomposition of the particles was observed in toluene up to 110 °C. Due to the boiling point of toluene (111 °C), a further increase in temperature was only possible by replacing toluene by *p*-xylene and indeed, a color change from brown-red to bluish accompanied by formation of a black precipitate was observed at 120 °C indicating thermal decomposition of the particles. The decompositions temperatures recorded for **Au-TPM-32** and **Au-TPM-64** were with 90 – 100 °C in a similar range as observed for **Au-TPM-8**.^[25] For both samples an initial increase of the SPR-band was observed at 100 °C pointing at the formation of larger agglomerates, followed by complete disappearance of the SPR-band at 110 °C due to crushing out of the Au(0) species. It is tempting to hypothesize that the stoichiometric match between two heptamers **TPM** per NP in **Au-TPM-16** is reflected in the increased thermal stability.

AuNPs stabilized by heptamer Ter

The NP syntheses in the presence of the heptamer **Ter** resembled the ones with **Xyl**. Also here major precipitations were detected during the syntheses even though the reaction solution remained red-colored. Interestingly, already the reaction with 8 equivalents of the gold salt featured a slight reddish hue, pointing towards larger AuNPs compared to previously reported NPs^[24–30], which themselves were - with 8 equivalents of gold-salt - dark brown in solution. It thus seems that the reaction conditions are not solely steering the dimensions of the NPs but that the chemical structure of the heptamer present has some influence as well. Despite all formed nanoparticles with this ligand were stable during the workup steps, they featured limited stability while drying and redispersing. While **Au-Ter-16**, **-32** and **-64**

were completely indispersible, **Au-Ter-8** showed only moderate redispersibility. Thus the characterization of these particles was limited to TEM analyses and UV-Vis spectroscopy.

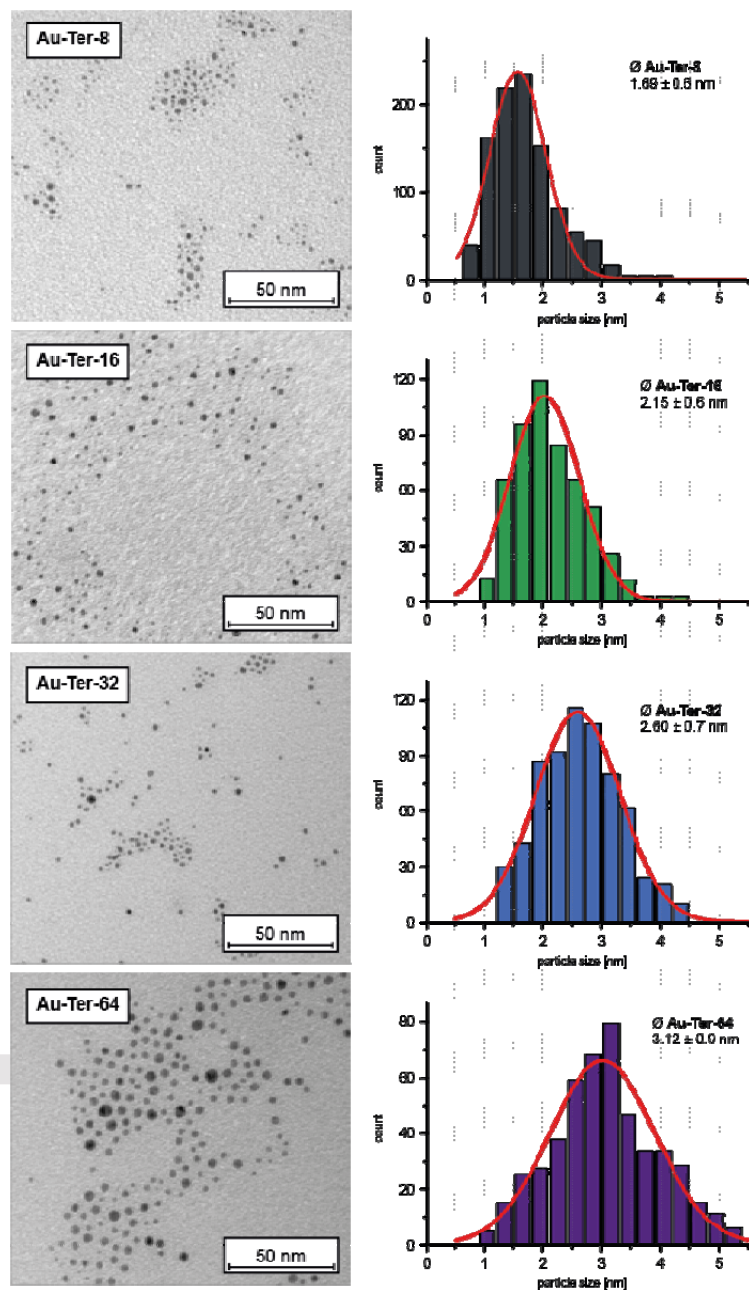


Figure 4: (Left) Representative sections of the TEM micrographs for samples of **Au-Ter-8**, **-16**, **-32** and **-64** and (right) their corresponding size distributions with calculated Gaussian curves (red). The vertical grid is implemented for better comparison.

The TEM investigations revealed sizes of 1.69 ± 0.6 nm for **Au-Ter-8**, 2.15 ± 0.6 nm for **Au-Ter-16**, 2.60 ± 0.7 nm for **Au-Ter-32**, and 3.12 ± 0.9 for **Au-Ter-64**. Again the trend to larger particles with an increased amount of gold salt used during their syntheses was observed for the terphenylic heptamer **Ter**. Interestingly the observed size increases with **Au-Ter-16** having a 1.27 times larger diameter than **Au-Ter-8**, **Au-Ter-32** with a 1.21 times the diameter of **Au-Ter-16**, and **Au-Ter-64** having 1.2 time the one of **Au-Ter-32** match almost perfectly the

increase by the factor $\sqrt[3]{2} = 1.26$ expected for the diameter upon doubling the mass of the particle. Compared to both other heptamer systems **Xyl** and **TPM**, which provided stable particles with a narrow size distribution when 8 equivalents of gold salt were used, the NPs obtained with **Ter** displayed limited stability features and were in general larger with broader size distributions, also if only 8 equivalents of

the gold salt were deployed. In spite of the two bulky *tert*-butyl groups, the heptamer **Ter** seems neither to be able to stabilize AuNPs of particular dimensions nor do these NPs display reasonable processability. We thus concluded that the structural motif is not suited for the development of functional coatings making NPs addressable by wet chemistry.

The UV-Vis spectra recorded for each heptamer system corroborate the size trends observed by TEM analyses and are displayed in figure 5 (AuNPs stabilized by **Xyl** (left), **TPM** (middle), and **Ter** (right)). For each ligand system a more prominent SPR-band was recorded the more gold-salt (8 eq., 16 eq., 32 eq., 64 eq. etc.) was used for the synthesis of the AuNPs. Also a slight red-shift^[2] of the SPR-band was observed for every ligand system when the obtained particles were getting larger. This effect is particularly apparent for the heptamer **TPM** due to the complementation of the series by **Au-TPM-512** and **Au-TPM-1024** to explore the limits of the stabilization potential of the ligand system. Eye catching is the increased size of **Au-Ter-8** (1.69 ± 0.6 nm) in the series of NPs synthesized with 8 equivalents of gold-salt (black lines), for which a SPR-band was visible, while **Au-Xyl-8** (1.15 ± 0.3 nm) and **Au-TPM-8** (1.17 ± 0.3 nm) did not display a SPR-band as expected for their tiny dimensions. While for thiolate-protected^[35-37] NPs typically stepwise UV-Vis absorption bands between 300 and 800 nm were observed within this minute size-regime, we do not observe similar bands in the UV-Vis for **Au-Xyl-8** and **Au-TPM-8**. This may either arise from the slightly broader size distribution^[38] and/or from the weaker thioether-gold interactions, as it is also reported for phosphine-stabilized^[39] NPs. For the next series of NPs synthesized with 16 equivalents of gold-salt (green line) a SPR-band was visible for all three members, even though the intensity of the band recorded for **Au-Xyl-16** (1.86 ± 0.6 nm) was unexpected weak considering the particles' sizes determined by TEM. AuNPs synthesized with 32 (blue lines) and 64 (purple lines) gold equivalents featured for every ligand system remarkable SPR-bands. Note that the shape of the SPR-band does not only depend on the particles' sizes but also on their shapes, morphologies, and their distributions.^[2]

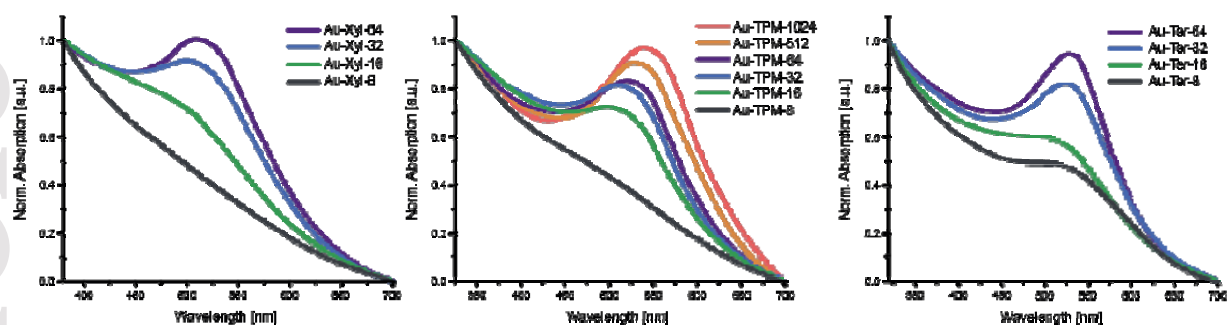


Figure 5: Normalized UV-Vis spectra of heptamers **Xyl** (left), **TPM** (middle) and **Ter** (right) stabilized AuNPs recorded in CH_2Cl_2 . Note that each molar gold equivalent features the same color code.

So far we have seen that for all three heptameric ligands investigated, with increasing amounts of gold-salt used the nanoparticles became larger, the size-distributions became broader, and their tendency to precipitate increased. There are however also clear differences mainly in the stability, solubility, and thus also processability of the heptamer coated particles and we wondered to which extent structural features of the ligands are reflected in the obtained NPs. Our initial working hypothesis was that an increased spacing between both sulfur atoms of a bridging motive might result in larger particles. The here investigated series of heptamers was an ideal model system to challenge this hypothesis, as the spacing between neighboring thioether sulfur atoms increases steadily from 4.6 Å for **Xyl**, over 9.6 Å for **TPM**, to 12 Å for **Ter**, as has been estimated from simple MM2 modeling. Figure 6 displays the recorded average particle's sizes of the AuNPs stabilized by the heptamers **Xyl**, **TPM**, and **Ter** with 8, 16, 32, and 64 equivalents of gold-salt used enabling the comparison of the NP dimensions between the different ligand systems.

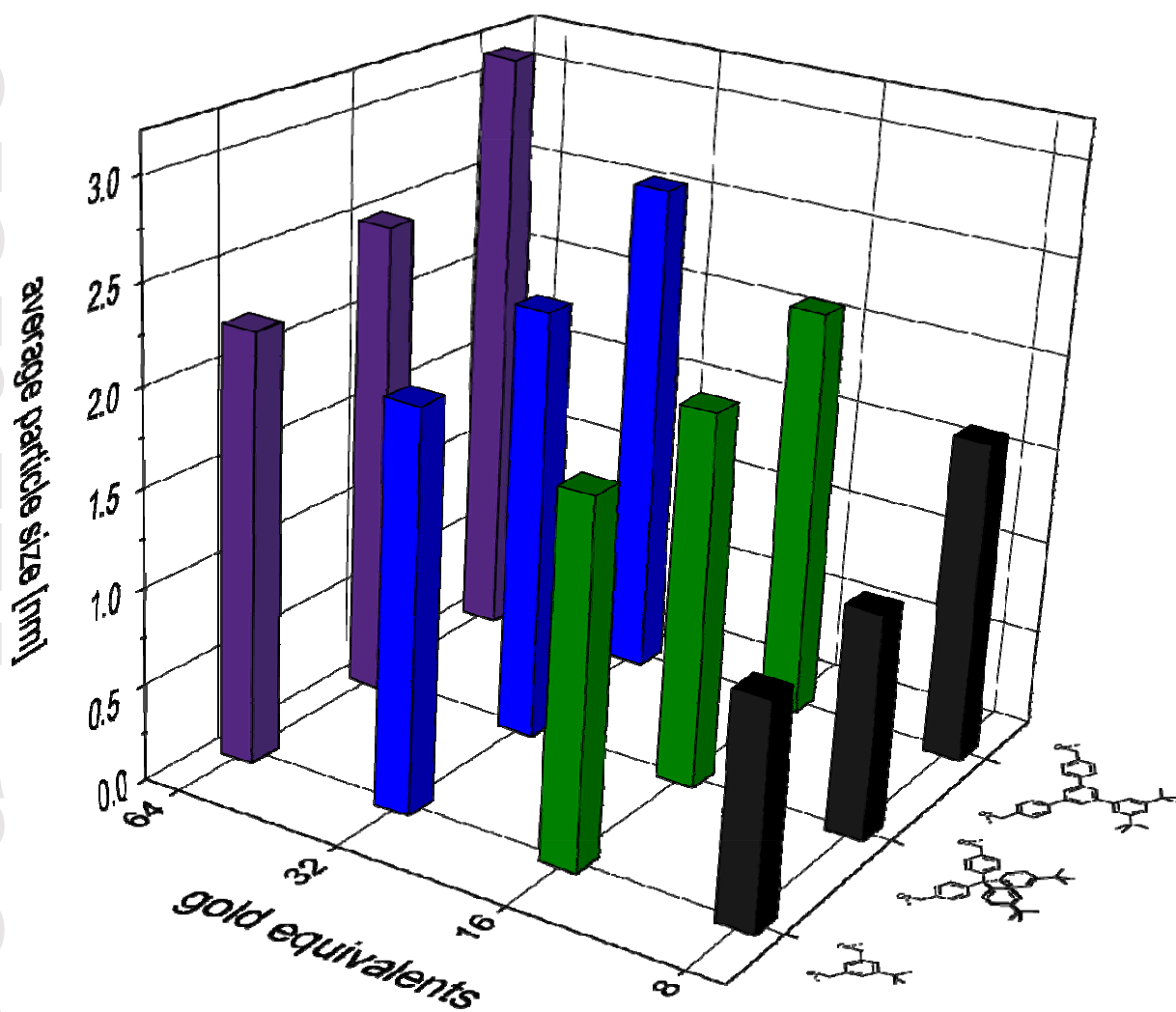


Figure 6: 3D-graph displaying the average sizes of AuNPs stabilized by heptamer **Xyl** (front row), **TPM** (middle row) and **Ter** (back row) synthesized from various amounts of gold salt. The color codes the gold equivalents used during the NP syntheses.

The 3D-graph clearly shows both trends, the increased dimensions of the particles due to the increased amount of gold present during the synthesis and the size increase due to the ligand structure used. While the order of the size increase due to the ligand structure supports the hypothesized correlation with the spacing between neighboring sulfur atoms, the amount of NP size increase is neither proportional to, nor another obvious function of the increase in S-S distance in the ligand system. It however remains questionable to which extent the dimensions of the NPs reflect directly structural features of the arrangement of the coating ligand at the NP surface or other physicochemical properties

depending on the coating like stability and solubility features influencing concentrations and growth kinetics. Eye-catching in the presentation of the entire collection of particles are the surprising small dimensions of the AuNPs synthesized from 8 equivalents of gold salt with the two heptamers **Xyl** and **TPM**. Both particles **Au-Xyl-8** and **Au-TPM-8** displayed good stability and processability features, were characterized by a narrow size distribution, and an integer average number of ligand per NP. It is thus tempting to interpret their small sizes as a consequence of a compact coating shell by 2 heptamers **Xyl** in the case of **Au-Xyl-8** and by a single molecule **TPM** in **Au-TPM-8**, as has already been reported.^[24,25] Also it is not surprising that the heptamer **Ter** is less suited to stabilize small particles, as the considerably increases S-S spacing results in more remote contact points disfavoring the adaption of the coating ligand shell to spherical objects with too small radii.

Conclusion

A systematic study identifying parameters and boundary conditions controlling the dimensions of ligand coated gold nanoparticles is presented. For that purpose, the series of heptameric ligand structures comprising eight benzylic thioether linkages as coordination site for the gold particles was complemented by the new ligand **Ter** with an increased distance between neighboring sulfur atoms in the ligand backbone. To enable quick access, the heptamer **Ter** was synthesized with an end-capping polymerization strategy in an isolated yield of 8%. The three linear heptameric ligand systems **Xyl**, **TPM**, and **Ter** were present during the reductions of various concentration of gold salts to investigate their AuNP stabilizing properties. For all three ligand systems the average sizes of the NPs grew with an increased concentration of the gold salt reduced. In addition, the sizes of the NPs also depends on the dimensions of the coating ligand with a trend reflecting the spacing between the sulfur atoms in the individual bridging motives. Also the different ligand motives displayed considerable differences in the stability and processability of the coated particles. While **Au-Xyl-q** only provided stable and redispersible NPs with low concentration of gold salt yielding in **Au-Xyl-8** with a well-defined ratio of two ligands coating the NP, larger amounts of gold salts provided larger NPs with reduced stability properties. All **Ter** coated particles (**Au-Ter-q**) only showed very limited stability and solubility features, while the entire **Au-TPM-q** series clearly displayed superior stability and processability properties compared to the other two ligand systems. It seems that the increased bulkiness of the bridging motive in **TPM** favors these desired physical-chemical characteristics.

We are currently further exploring this motive in dendritic structures in order to obtain well coated, stable NPs which are large enough for optical applications.

Acknowledgements

We thank the Swiss National Science Foundation (Grant No. 200020_159730) for financial support.

Supporting Information ^1H -NMR of **Au-TPM-16**, **-32**, **-64**, representative TEM images, UV-Vis traces of thermal stability measurements, thermogravimetric analysis, NMR spectra (^1H , ^{13}C), elemental analysis and high-resolution mass traces.

Experimental Section

Instruments and Materials

All commercially available starting materials were of reagent grade and used as received, unless stated differently. Absolute tetrahydrofuran (THF), dimethyl sulfoxide (DMSO) and dichloromethane (DCM) were purchased from *Acros Organics*, stored over 4Å molecular sieves, and handled under argon. *tert*-Butylmethylether (MTBE), *c*-hexane, ethyl acetate (EtOAc) and dichloromethane were used for purification and were of technical grade. Column chromatography purifications were carried out on *SilicaFlash® P60* (particle size 40 - 63 µm) from *SiliCycle*. Deuterated solvents were purchased from *Cambridge Isotope Laboratories*. ^1H - and ^{13}C -NMR spectra were recorded with a *Bruker DPX 400* instrument (^1H resonance 400 MHz) or a *Bruker DRX 500* instrument (^1H resonance 500 MHz) at 298 K. The chemical shifts (δ) are reported in ppm and are referenced to the residual proton signal of the deuterated solvent (CDCl_3 : 7.26 ppm) for ^1H spectra or the carbon of the solvent (CDCl_3 : 77.0 ppm) for ^{13}C spectra. The coupling constants (J) are given in Hertz (Hz), the multiplicities are denoted as: *s* (singlet), *d* (duplet), *t* (triplet), *m* (multiplet) and *br* (broad). MALDI-ToF mass spectra were performed on a *Bruker microflex™* mass spectrometer, calibrated with CsI_3 , and α -cyano-4-hydroxycinnamic acid (unless stated differently) was used as matrix. Important signals are given in *m/z*. Gas chromatography-mass spectrometry (GC-MS) was performed on a *Shimadzu GCMS-QP2010 SE* gas chromatography system with a ZB-5HT inferno column (30 m x 0.25 m x 0.25 m), at 1 ml/min He-flow rate (split =20:1)

This article is protected by copyright. All rights reserved.

with a *Shimadzu* mass detector (EI 70 eV). DART-MS was measured on a IonSense DART-SVP100 (He, 450 °C) connected to a *Shimadzu* LC-2020. High-resolution mass spectra (HRMS) were measured as HR-ESI-ToF-MS with a *Bruker* Maxis 4G instrument or HR-MALDI-FTICR with a *Bruker* solariX 94. Gel permeation chromatography (GPC) for the purification of gold nanoparticles was performed manually using *Bio-Rad Bio-Beads S-X1* (operating range 600-14'000 g/mol) with dichloromethane as solvent. For purification of the ligands a (automated) *Shimadzu Prominence System* was used with SDV preparative columns from *Polymer Standards Service* (two Showdex columns in series, 20 mm x 600 mm each, exclusion limit: 30'000 g/mol) with chloroform as solvent. UV-Vis measurements was performed on a *Shimadzu UV spectrometer UV-1800* using optical 1115F-QS *Hellma* cuvettes (10 mm light path). Elemental analysis (EA) was performed by Sylvie Mittelheisser on a *Vario Micro Cube*. Transmission electron microscopy (TEM) was performed on a *Philips CM100* transmission electron microscope at 80 kV using copper grids (Cu-400HD) from *Pacific Grid Tech*.

3,5-Dibromo-3',5'-di-tert-butyl-1,1'-biphenyl (4): 1,3-Dibromo-5-iodobenzene 5.84 g, 16.1 mmol), 1,3-di-tert-butylphenyl boronic acid (3.97 g, 17 mmol) and potassium carbonate (13.5 g, 96.9 mmol) were subsequently added to a 1000 ml argon-purged two-neck flask. Toluene (500 ml) and water (100 ml) were added and the reaction mixture was degassed with argon for 15 minutes. Pd(PPh₃)₄ (377 mg, 0.323 mmol) was added and the mixture was refluxed for 15 hours. The resulting mixture was poured into water and extracted 3 times with EtOAc. The combined organic fractions were dried over magnesium sulfate (MgSO₄), filtrated and the volatile was evaporated to dryness. The yellow solid was subjected to column chromatography on silica eluting with *c*-hexane/DCM (10:1) yielding compound **4** as a white solid (5.80 g, 85 %). ¹H NMR (400 MHz, Chloroform-*d*) δ 7.63 (s, 3H), 7.48 (t, *J* = 1.8 Hz, 1H), 7.32 (d, *J* = 1.8 Hz, 2H), 1.38 (s, 18H). ¹³C NMR (101 MHz, CDCl₃) δ 151.59, 146.14, 137.90, 132.25, 129.25, 123.08, 122.60, 121.54, 35.03, 31.49. GC-MS (EI, 70 eV): *m/z* (%) = 57.1 (100), 409 (32), 411 (16), 407 (15), 424.05 (8), 89.05 (7), 410 (6), 103.1 (5), 426 (5), 422.05 (5), 58.1 (4), 101.1 (4), 94.6 (4), 408.05 (4), 412 (3), 142.6 (3), 102.05 (3), 191.1 (3), 55.1 (3). EA: found: C 56.89 %, H 5.53 %; required: C 56.63 %, H 5.70 %.

3,5-Di-tert-butyl-4''-methyl-5'-(*p*-tolyl)-1,1':3',1''-terphenyl (3): Compound **4** (119 mg, 0.28 mmol), *p*-tolylboronic acid (102 mg, 0.72 mmol) and potassium carbonate (235 mg, 1.68 mmol) were subsequently added to a 50 ml argon-purged two-neck flask. Tetrahydrofuran (25 ml) and water (5 ml)

This article is protected by copyright. All rights reserved.

were added and the reaction mixture was degassed with argon for 15 minutes. Pd(PPh₃)₄ (32.7 mg, 0.02 mmol) was added and the mixture was refluxed for 15 hours. The resulting mixture was poured into water and extracted 3 times with EtOAc. The combined organic fractions were dried over MgSO₄, filtrated and the volatile was evaporated to dryness. The yellow solid was subjected to column chromatography on silica eluting with *c*-hexane to afford a white solid (**3**) (112.6 mg, 90 %). ¹H NMR (400 MHz, Chloroform-*d*) δ 7.74 (dd, *J* = 7.6, 1.7 Hz, 3H), 7.63 – 7.59 (m, 4H), 7.51 – 7.48 (m, 3H), 7.33 – 7.29 (m, 4H), 2.43 (s, 6H), 1.40 (s, 18H). ¹³C NMR (101 MHz, CDCl₃) δ 151.21, 143.69, 142.12, 140.87, 138.53, 137.27, 129.56, 127.27, 125.20, 124.66, 121.93, 121.63, 35.03, 31.57, 21.16. HRMS (MALDI-ToF): measured: *m/z* 446.2968, 469.2866 ([M+Na]⁺), 485.2605 ([M+K]⁺); calculated: *m/z* 446.2968, 469.2866 ([M+Na]⁺), 485.2605 ([M+K]⁺).

4''-(Bromomethyl)-5'-(4-(bromomethyl)phenyl)-3,5-di-*tert*-butyl-1,1':3',1''-terphenyl (2): Compound **3** (3.91 g, 8.75 mmol) and N-bromosuccinimide (6.29 g, 35 mmol) were added to an argon-purged 500 ml three-neck flask and suspended in methyl formate (250 ml) and degassed with argon for 20 minutes. After addition of AIBN (147 mg, 0.87 mmol) the reaction mixture was illuminated by a 500 W halogen lamp and refluxed over night. The solvent was removed by distillation and the residue was redissolved in DCM. The mixture was washed once with a saturated aqueous solution of Na₂S₂O₃, twice with a saturated aqueous solution of NaHCO₃, once with water and brine. The organic phase was dried over MgSO₄, filtrated and the solvent was removed *in vacuo*. The residue was subjected to column chromatography eluting with *c*-hexane/DCM (10:1) to afford compound **2** as a white solid (4.78 g, 90 %). ¹H NMR (400 MHz, Chloroform-*d*) δ 7.76 – 7.72 (m, 3H), 7.69 – 7.64 (m, 4H), 7.54 – 7.47 (m, 7H), 4.58 (s, 4H), 1.40 (s, 18H). ¹³C NMR (101 MHz, CDCl₃) δ 151.51, 144.11, 144.06, 141.72, 141.52, 140.61, 137.27, 129.76, 127.97, 125.95, 124.98, 122.01, 35.19, 33.44, 31.70. HRMS (MALDI-ToF): measured: *m/z* 601.1099; calculated: *m/z* 601.1100.

(5'-(3,5-Di-*tert*-butylphenyl)-[1,1':3',1''-terphenyl]-4,4''-diyl)dimethanethiol (1): A solution of **2** (1 g, 1.65 mmol) and thiourea (0.63 g, 8.27 mmol) in dry dimethyl sulfoxide (10 ml) was left stirring for 15 hours at 40 °C under an atmosphere of argon. The mixture was diluted with DCM (50 ml) and the formed white precipitate (isothiuronium salt) filtrated and washed with additional DCM. The white solid was added into a 1 L round bottom flask, purged with argon and dissolved in methanol (200 ml). The reaction mixture was bubbled with argon for 30 minutes and then a degassed aqueous solution of 1

M NaOH (200 ml) was added into the reaction mixture and stirred for 1.5 hours. Then, a degassed aqueous solution of 1 M HCl (250 ml) was added and stirred for 1.5 hours. The reaction mixture was washed three times with DCM (3x150 ml). The combined organic phases were dried over MgSO₄, filtrated and the volatile was removed *in vacuo* to afford compound **1** as white solid (420 mg, 56 %). ¹H NMR (400 MHz, Chloroform-*d*) δ 7.75 (s, 3H), 7.67 (d, *J* = 8.2 Hz, 4H), 7.56 – 7.42 (m, 7H), 3.83 (d, *J* = 7.6 Hz, 4H), 1.84 (t, *J* = 7.6 Hz, 2H), 1.42 (s, 18H). ¹³C NMR (101 MHz, CDCl₃) δ 151.32, 143.86, 141.81, 140.65, 140.54, 140.11, 128.59, 127.72, 125.55, 124.78, 121.90, 121.78, 35.06, 31.59, 28.73. HRMS (MALDI-ToF): measured: *m/z* 509.2332 ([M-1H]⁻), 508.2253 ([M-2H]⁻); calculated: *m/z* 509.2331 ([M-1H]⁻), 508.2253 ([M-2H]⁻).

Heptamer Ter: For the “end-capping oligomerization” reaction, compound **2** (18.6 mg, 30.7 μmol) and **1** (19.6 mg, 38.4 μmol) were dissolved in freshly distilled and degassed THF (3 ml) and the reaction mixture was degassed with argon for 10 minutes. The oligomerization was initiated by addition of sodium hydride (12.3 mg, 307 μmol) and let react for 15 minutes at room temperature, after which 4-methylbenzyl bromide (23.4 mg, 123 μmol) was added. After 15 hours, the reaction mixture was quenched by addition of water, extracted with methyl *tert*-butyl ether (MTBE) (3 x 10 ml) and dried with MgSO₄. The volatile was removed *in vacuo* and the crude product was subjected to a short column chromatography eluting with *c*-hexane/EtOAc (1:1) and then purified on automated recyclable GPC yielding heptamer **Ter** as colorless oil (2.8 mg, 8 %). ¹³C NMR (101 MHz, CDCl₃) δ 151.28, 143.84, 141.81, 140.68, 140.05, 137.50, 129.55, 129.51, 129.19, 128.91, 127.52, 127.45, 125.48, 124.75, 121.88, 121.74, 35.41, 35.38, 35.26, 35.03, 31.57. ¹H NMR (400 MHz, Chloroform-*d*) δ 7.78 – 7.74 (m, 22H), 7.70 – 7.66 (m, 24H), 7.50 – 7.48 (m, 26H), 7.45 (d, *J* = 8.2 Hz, 26H), 3.72 (s, 24H), 3.65 (s, 4H), 3.62 (s, 4H), 2.34 (s, 6H), 1.40 (s, 126H). HRMS (MALDI-ToF): measured: 3598.8740 ([M+Na]⁺), 3614.8480 ([M+K]⁺); calculated: 3598.8785 ([M+Na]⁺), 3614.8525 ([M+K]⁺).

General procedure for gold nanoparticle formation and purification

Gold nanoparticle syntheses were carried out on a 10 - 50 μmol scale with respect to the molar ligand equivalents. For each heptamer (1 molar equivalent) a series of 8, 16, 32 and 64 molar equivalents of tetrachloroauric acid was used for the formation of AuNPs (for heptamer **TPM** even 512 and 1024 molar equivalents). Tetrachloroauric acid was dissolved in 2.5 ml deionized water. A solution of tetraoctylammonium bromide (2 times Au equivalents) in 2.5 ml DCM was added and the two-phase mixture stirred until the aqueous phase became colourless. The ligand (1 equivalent) was dissolved in

2.5 ml dichloromethane and then added to the reaction mixture, and let stir for 15 minutes, allowing the thioether moieties and the gold to pre-organize their conformation. A freshly prepared solution of sodium borohydride in 2.5 ml of water was then added quickly to the reaction mixture. After 10 min stirring, the resulting strongly coloured dichloromethane phase was separated and the aqueous phase was washed twice with dichloromethane. The combined organic fractions were concentrated to a volume of *ca.* 0.5 - 1 ml. Approx. 20 ml ethanol was added to precipitate the particles, which were then centrifuged. The supernatant was discarded and the procedure was repeated twice.

References

- [1] M. Brust, M. Walker, D. Bethell, D. J. Schiffrin, R. Whyman, *J. Chem. Soc. Chem. Commun.* **1994**, 801–802.
- [2] P. Zhao, N. Li, D. Astruc, *Coord. Chem. Rev.* **2013**, *257*, 638–665.
- [3] M.-C. Daniel, D. Astruc, *Chem. Rev.* **2004**, *104*, 293–346.
- [4] R. Jin, *Nanoscale* **2010**, *2*, 343–362.
- [5] D. A. Tomalia, S. N. Khanna, *Chem. Rev.* **2016**, *116*, 2705–2774.
- [6] G. Schmid, U. Simon, *Chem. Commun.* **2005**, 697–710.
- [7] N. Bodappa, U. Fluch, Y. Fu, M. Mayor, P. Moreno-García, H. Siegenthaler, T. Wandlowski, *Nanoscale* **2014**, *6*, 15117–15126.
- [8] R. Liffmann, M. Homberger, M. Mennicken, S. Karthäuser, U. Simon, *RSC Adv.* **2015**, *5*, 102981–102992.
- [9] F. Kretschmer, S. Mühlig, S. Hoepfener, A. Winter, M. D. Hager, C. Rockstuhl, T. Pertsch, U. S. Schubert, *Part. Part. Syst. Charact.* **2014**, *31*, 721–744.
- [10] K. Saha, S. S. Agasti, C. Kim, X. Li, V. M. Rotello, *Chem. Rev.* **2012**, *112*, 2739–2779.
- [11] L.-Y. Chen, C.-W. Wang, Z. Yuan, H.-T. Chang, *Anal. Chem.* **2015**, *87*, 216–229.
- [12] M. M. Alvarez, J. T. Khoury, T. G. Schaaff, M. N. Shafiqullin, I. Vezmar, R. L. Whetten, *J. Phys. Chem. B* **1997**, *101*, 3706–3712.
- [13] M. J. Hostetler, J. E. Wingate, C.-J. Zhong, J. E. Harris, R. W. Vachet, M. R. Clark, J. D. Londono, S. J. Green, J. J. Stokes, G. D. Wignall, et al., *Langmuir* **1998**, *14*, 17–30.
- [14] T. Chen, Z. Luo, Q. Yao, A. X. H. Yeo, J. Xie, *Chem. Commun.* **2016**, *52*, 9522–9525.

- [15] S. M. Ansar, F. S. Mohammed, G. von White, M. Budi, K. C. Powell, O. T. Mefford, C. L. Kitchens, *J. Phys. Chem. C* **2016**, *120*, 6842–6850.
- [16] S. R. K. Perala, S. Kumar, *Langmuir* **2013**, *29*, 9863–9873.
- [17] I. Hussain, S. Graham, Z. Wang, B. Tan, D. C. Sherrington, S. P. Rannard, A. I. Cooper, M. Brust, *J. Am. Chem. Soc.* **2005**, *127*, 16398–16399.
- [18] Z. Wang, B. Tan, I. Hussain, N. Schaeffer, M. F. Wyatt, M. Brust, A. I. Cooper, *Langmuir* **2007**, *23*, 885–895.
- [19] M. Azubel, R. D. Kornberg, *Nano Lett.* **2016**, DOI 10.1021/acs.nanolett.6b00981.
- [20] E. W. Elliott, P. M. Haben, J. E. Hutchison, *Langmuir* **2015**, *31*, 11886–11894.
- [21] R. McCaffrey, H. Long, Y. Jin, A. Sanders, W. Park, W. Zhang, *J. Am. Chem. Soc.* **2014**, *136*, 1782–1785.
- [22] B. Mondal, K. Acharyya, P. Howlader, P. S. Mukherjee, *J. Am. Chem. Soc.* **2016**, *138*, 1709–1716.
- [23] A. Uehara, S. G. Booth, S. Y. Chang, S. L. M. Schroeder, T. Imai, T. Hashimoto, J. F. W. Mosselmans, R. A. W. Dryfe, *J. Am. Chem. Soc.* **2015**, *137*, 15135–15144.
- [24] T. Peterle, A. Leifert, J. Timper, A. Sologubenko, U. Simon, M. Mayor, *Chem. Commun.* **2008**, 3438–3440.
- [25] M. Lehmann, E. H. Peters, M. Mayor, *Chem. – Eur. J.* **2016**, *22*, 2261–2265.
- [26] J. P. Hermes, F. Sander, T. Peterle, R. Urbani, T. Pfohl, D. Thompson, M. Mayor, *Chem. – Eur. J.* **2011**, *17*, 13473–13481.
- [27] J. P. Hermes, F. Sander, U. Fluch, T. Peterle, D. Thompson, R. Urbani, T. Pfohl, M. Mayor, *J. Am. Chem. Soc.* **2012**, *134*, 14674–14677.
- [28] F. Sander, U. Fluch, J. P. Hermes, M. Mayor, *Small* **2014**, *10*, 349–359.
- [29] T. Peterle, P. Ringler, M. Mayor, *Adv. Funct. Mater.* **2009**, *19*, 3497–3506.
- [30] J. P. Hermes, F. Sander, T. Peterle, C. Cioffi, P. Ringler, T. Pfohl, M. Mayor, *Small Weinh. Bergstr. Ger.* **2011**, *7*, 920–929.
- [31] M. Sakamoto, D. Tanaka, T. Teranishi, *Chem. Sci.* **2012**, DOI 10.1039/C2SC21560H.
- [32] MM2 Calculations in Chem3D, **n.d.**
- [33] P. Lustenberger, F. Diederich, *Helv. Chim. Acta* **2000**, *83*, 2865–2883.
- [34] K. G. Thomas, J. Zajicek, P. V. Kamat, *Langmuir* **2002**, *18*, 3722–3727.

- [35] R. L. Donkers, D. Lee, R. W. Murray, *Langmuir* **2004**, *20*, 1945–1952.
- [36] V. L. Jimenez, D. G. Georganopoulou, R. J. White, A. S. Harper, A. J. Mills, D. Lee, R. W. Murray, *Langmuir* **2004**, *20*, 6864–6870.
- [37] M. Walter, J. Akola, O. Lopez-Acevedo, P. D. Jadzinsky, G. Calero, C. J. Ackerson, R. L. Whetten, H. Grönbeck, H. Häkkinen, *Proc. Natl. Acad. Sci.* **2008**, *105*, 9157–9162.
- [38] M. Zhu, E. Lanni, N. Garg, M. E. Bier, R. Jin, *J. Am. Chem. Soc.* **2008**, *130*, 1138–1139.
- [39] W. W. Weare, S. M. Reed, M. G. Warner, J. E. Hutchison, *J. Am. Chem. Soc.* **2000**, *122*, 12890–12891.